A Peculiar Photo-Induced Transformation Exalted in Nanometric Size CoFe Prussian Blue Analogs

Grégory A Balthazar, Amélie Bordage, Giulia Fornasieri, Laura Altenschmidt, Andrea Zitolo, Anne Bleuzen

ChemPhotoChem

Research Articles
doi.org/10.1002/cptc.202300102

Chemistry Europe
European Chemical Societies Publishing

www.chemphotochem.org

A Peculiar Photo-Induced Transformation Exalted in Nanometric Size CoFe Prussian Blue Analogs

Grégory Balthazar,[a] Amélie Bordage,[a] Giulia Fornasieri,[a] Laura Altenschmidt,[a] Andrea Zitolo,[b] and Anne Bleuzen*[a]

The discovery of a photomagnetic effect in a CoFe Prussian blue analog (PBA) has triggered a growing interest for photo-switchable bimetallic cyanide-bridged systems. Nevertheless, in between cyanide-bridged extended coordination polymers and discrete molecules, the photo-switching phenomena are much less well known in nano-sized materials. A photo-induced transformation, specific to the nanometric size, is evidenced by magnetometry and by X-ray absorption spectroscopy at the Co and Fe K-edges in an alkali cation free Prussian blue analog. The nanoparticles before irradiation can be described as having a core-shell structure, the core being made of the well-known fcc-$Co^{II}(HS)Fe^{III}$ structure of CoFe PBAs while the shell contains Co^{II} ions in octahedral geometry and significantly distorted $Fe(CN)_6$ entities. Irradiation induces a change of the local structures around the transition metal ions, which remain in the same oxidation state, with different behaviors of the Co and Fe sub-lattices.

Introduction

The discovery in 1991 of a photomagnetic effect in a CoFe Prussian Blue Analog[1] (PBA) has triggered a growing interest for photo-switchable bimetallic cyanide-bridged systems. Switchable, and especially photo-switchable, molecular materials associated with very short addressing times being promising candidates for the preparation of memory and multifunctional devices, a wide range of photo-switchable cyanide-bridged coordination polymers[2] and molecules[3] were and are still prepared and studied. These compounds, prepared in the form of monocrystals or powders, actively participate to the thorough understanding of the photo-switching phenomena in these systems. In CoFe PBAs and derived molecules, it is now well established that photo-switching is due to a combined $Co^{III}(LS)Fe^{II} \rightarrow Co^{II}(HS)Fe^{III}$ electron transfer and spin conversion of the Co ion, accompanied with a significant unit cell volume expansion.[4]

In between cyanide-bridged extended coordination polymers (among them PBAs having the well-known fcc structure[5]) and the discrete molecules, the photo-switching phenomena are much less well known in nanosized particles. Photo-switching properties have been evidenced in some nanosized systems,[6] but the mechanisms involved in their photo-switching properties[7] and the effects of size reduction on them[8] have been very little explored. The poor knowledge of photo-switching phenomena in nanosized systems stems from the difficulty of controlling both the chemical composition governing the photo-switching properties and the size of the nanoparticles, which is a prerequisite to the thorough study of such systems. Indeed, the control of both nucleation-growth and chemical composition goes through a fine but most often different control of the reaction medium, which makes very tricky the preparation of nanoparticles with both controlled size and chemical composition.

In order to control both the size and the chemical composition of PBA nanoparticles, our team developed an original approach using ordered mesoporous silica monoliths as chemically inert nanoreactors to confine the PBAs growth. Monocrystalline PBA nanoparticles embedded in the silica matrix, the size and chemical composition of which are determined by the diameter of the pores and the chemical composition of the reaction medium in the pores respectively, are thus obtained.[9] As CoFe PBA powders (made of particles having larger size, typically around 100 nm) prepared in the presence of an excess of Rb^+ cations exhibit an important photomagnetic effect,[2a] this approach was used to prepare CoFe PBA nanoparticles in the presence of an excess of Rb^+ cations. The 5 nm nanocrystals thus obtained exhibit a photomagnetic effect and are called **NanoRbCoFe** in the following.[8,10] An X-ray Absorption Spectroscopy (XAS) investigation[8] allowed us to evidence a core-shell structure of the nanocrystals in their ground state. The structure and electronic structure of the core are very close to that of the counterpart larger fcc-$Co^{III}(LS)Fe^{II}$ particles. The shell, made of two to three metallic layers, is composed of $Co^{II}(HS)$ ions in octahedral geometry and $Fe(CN)_6$ entities with a peculiar

[a] G. Balthazar, Dr. A. Bordage, Dr. G. Fornasieri, Dr. L. Altenschmidt, Prof. Dr. A. Bleuzen
Institut de Chimie Moléculaire et des Matériaux d'Orsay
Université Paris-Saclay, CNRS
Bâtiment Henri Moissan, 19 avenue des Sciences, 91400 Orsay, France
E-mail: anne.bleuzen@universite-paris-saclay.fr
[b] Dr. A. Zitolo
Synchrotron SOLEIL
L'Orme des Merisiers, St Aubin, BP 48, 91192 Gif sur Yvette, France

Supporting information for this article is available on the WWW under https://doi.org/10.1002/cptc.202300102

distorted structure. The fcc-$Co^{III}(LS)Fe^{II}$ core is photo-switchable and the $Co^{III}(LS)Fe^{II} \rightarrow Co^{II}(HS)Fe^{III}$ photo-induced electron transfer is similar to that observed in the larger particles. Intriguingly, the core-shell structure vanishes in the photo-excited state of **NanoRbCoFe**, meaning that the shell of **NanoRbCoFe** also undergoes a light-induced transformation, which can be either the consequence of the volume increase of the core accompanying the photo-induced $Co^{III}(LS)Fe^{II} \rightarrow Co^{II}(HS)Fe^{III}$ electron transfer or one other photo-induced transformation specific to the shell species and/or to nanosized particles.

With the aim to better understand this photo-induced transformation specific to nanosized systems, we synthesized PBA nanocrystals counterparts of the alkali cation free CoFe PBA powder, which is known to be made of the $Co^{II}(HS)Fe^{III}$ pairs and not photo-switchable. In order to prevent insertion of alkali cations and the formation of a few photo-switchable $Co^{III}(LS)Fe^{II}$ pairs, we replaced the $K_3[Fe(CN)_6]$ source of $[Fe(CN)_6]^{3-}$ complexes by $H_3[Fe(CN)_6]$. Alkali cation free nanocrystals (called **NanoH_CoFe** in the following) and the corresponding powder made of larger size particles (called **H_CoFe** in the following) were thus prepared and their sensitivity to light was investigated by magnetometry and by XAS.

Results and Discussion

The Field Cooled (FC) and Zero Field Cooled (ZFC) magnetization curves of **NanoH_CoFe** and **H_CoFe** were recorded before and after irradiation. They are shown in Figure 1. The irradiation conditions with a laser diode in the SQUID magnetometer were those optimized for the study of photomagnetic PBA powders in order to compare the behaviors of the nanocomposite and the powder in the same irradiation conditions.

Figure 1b shows that the ZFC and FC curves of **H_CoFe** before and after irradiation are very close. **H_CoFe** is very little sensitive to the visible light. Indeed, **H_CoFe** does not contain or contains only very few $Co^{III}(LS)Fe^{II}$ pairs, responsible for the photomagnetic effect in the CoFe PBAs and derivatives. In contrast, the FC and ZFC magnetization curves of **NanoH_CoFe** (Figure 1a) are significantly different before and after irradiation, showing a photo-transformation of the sample under visible-light irradiation. This shows that **NanoH_CoFe** is photo-excited towards a state, which is trapped with a long lifetime at low temperature. The temperature dependences of the magnetization of **NanoH_CoFe** before and after irradiation and their difference (S1) show that the initial magnetization is recovered after thermal treatment at 110 K, showing that the photo-induced transformation is reversible through thermal relaxation and/or thermal annealing. Such a transformation under irradiation was unexpected for **NanoH_CoFe** since the characterization of the nanocomposite does not evidence the presence of photo-switchable $Co^{III}(LS)Fe^{II}$ pairs in the CoFe PBA nanoparticles present in **NanoH_CoFe** (S2–S4). This surprising result evidenced by magnetometry after irradiation by visible light add to the surprising result evidenced for **NanoRbCoFe** by XAS after irradiation by the X-ray beam described in the introduction part.[8] This again suggests a peculiar and more complex behavior of nanosized systems under irradiation.

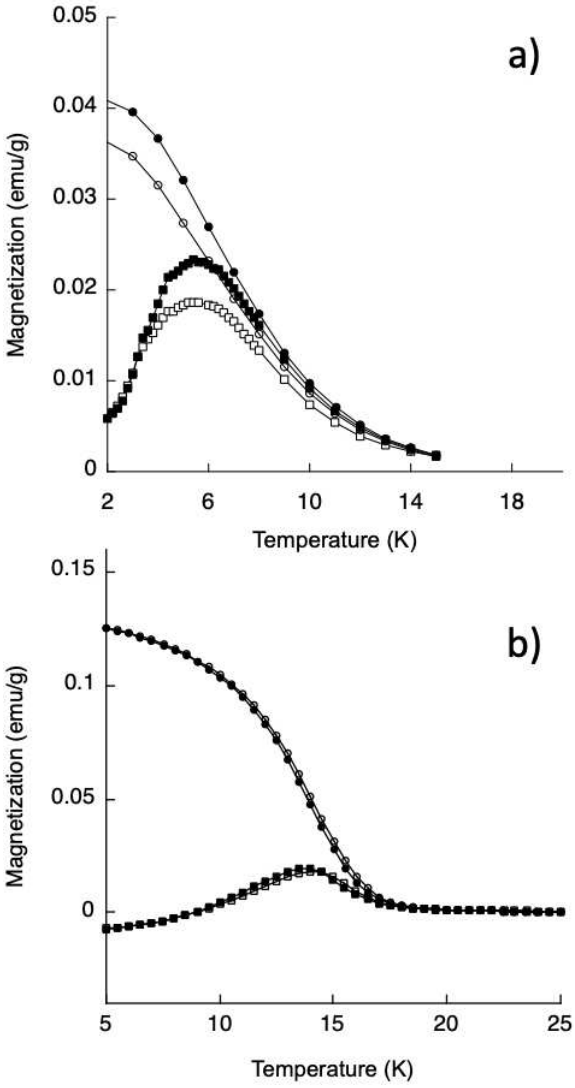

Figure 1. a) FC (circles) and ZFC (squares) mass magnetization curves before (white) and after (black) irradiation (635 nm, 25 mW/cm^2) for a) **NanoH_CoFe** and b) **H_CoFe**.

In order to get a better insight into photo-switching at the nanoscale in CoFe PBAs, we investigated **NanoH_CoFe** by X-Ray Absorption Spectroscopy (XAS) at the Co and Fe K-edges before and after irradiation. The XAS spectra of **H_CoFe**, as a model of the fcc-$Co^{II}(HS)Fe^{III}$ state, were recorded in the same experimental conditions for comparison.

The X-ray absorption spectra at the Co and Fe K-edges of **NanoH_CoFe** and of **H_CoFe** recorded at room temperature are displayed in Figure 2. The spectra of **H_CoFe** are characteristic of the $Co^{II}(HS)$ ions in an octahedral environment and of the $Fe^{III}(CN)_6$ entities of the fcc-$Co^{II}(HS)Fe^{III}$ state of large size CoFe PBA particles.[2a,4a,12] At the Co K-edge, the spectrum of **NanoH_CoFe** is very close to that of **H_CoFe**, showing that **NanoH_CoFe** contains $Co^{II}(HS)$ ions in octahedral geometry very close to those present in **H_CoFe**. Only the weak shoulder above the absorption maximum (7729 eV) indicates a slight

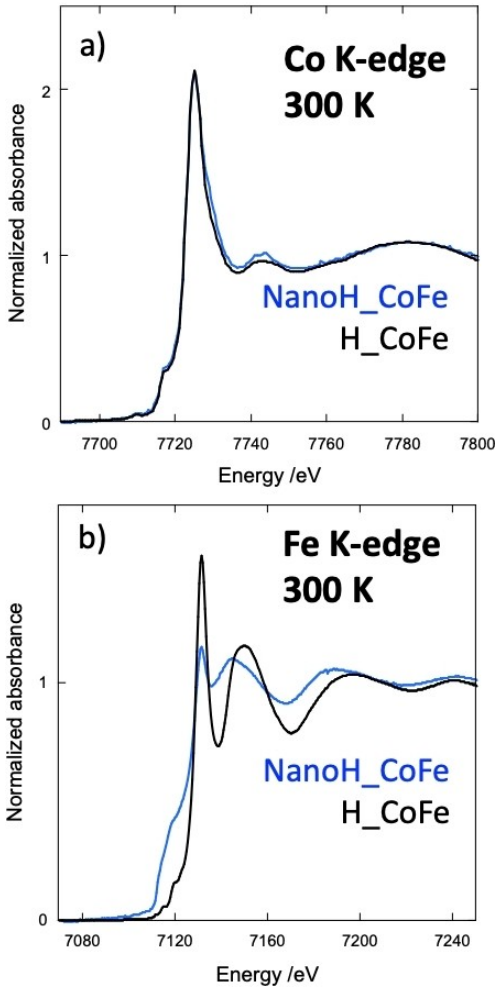

Figure 2. Room temperature XANES spectra of **NanoH_CoFe** (blue) and **H_CoFe** (black) a) at the Co K-edge and b) at the Fe K-edge.

difference of the Co sites in both compounds. Nevertheless, one can conclude that the Co sublattice is much the same in both compounds. At the Fe K-edge, the absorption maximum is located at the same energy on the spectra of **NanoH_CoFe** and of **H_CoFe** (7131 eV), but the shape of the spectra strongly differs; this reflects the same oxidation state of the Fe ions but strong differences of their local structure in both compounds. Such shape of the spectra at the Co and Fe K-edges is reminiscent of that of **NanoRbCoFe** in ref. [8], where we showed that the spectra of the latter can be decomposed into the spectra of a fcc-CoFe PBA core and of a shell with a peculiar structure. Therefore, the same data treatment as was used in ref. [8] was applied here to extract the spectra of species at both K-edges, which could constitute the core and the shell of **NanoH_CoFe**. For the sake of simplicity, the two contributions will also be called Core and Shell here; this will be discussed in the following. Thus, the XAS spectra of **NanoH_CoFe** are compared to those of model compounds: **H_CoFe** as a model of fcc-$Co^{II}(HS)Fe^{III}$, **H_RbCoFe** as a model of fcc-$Co^{III}(LS)Fe^{II}$ and **NanoH_RbCoFe** as a model of shell species surrounding a fcc-$Co^{III}(LS)Fe^{II}$ core. The syntheses of **H_RbCoFe** and **NanoH_RbCoFe** are presented in the experimental section and their characterizations in S2, S3 and S4.

Linear combinations of the spectra of **H_CoFe** and **NanoH_CoFe** on the one hand and of **H_RbCoFe** and **NanoH_RbCoFe** on the other hand enabled to extract the contribution of the shell of **NanoH_CoFe** (called **ShellNanoH_CoFe**) and of **NanoH_RbCoFe** (called **ShellNanoH_RbCoFe**), as well as the core ones (respectively called **CoreNanoH_CoFe** and **CoreNanoH_RbCoFe**). The extraction is based on the assumption that, if **NanoH_CoFe** and **NanoH_RbCoFe** have indeed a core-shell structure, their spectra is the combination of the contributions of the shell and of the core, the spectra of the core being identical to those of the powdered compounds (**H_CoFe** and **H_RbCoFe**) made of particles hundreds of nm in size as we observed in ref [8]. Therefore, the 1st step of the extraction consisted in a systematic linear combination by step of 10% of **H_CoFe** and **NanoH_CoFe** on the one hand, and **H_RbCoFe** and **NanoH_RbCoFe** on the other hand using Equations (1) and (2):

$$\mu_{NanoH\_CoFe} = x\mu_{H\_CoFe} + (1-x)\mu_{ShellNanoH\_CoFe} \quad (1)$$

$$\mu_{NanoH\_RbCoFe} = y\mu_{H\_RbCoFe} + (1-y)\mu_{ShellNanoH\_RbCoFe} \quad (2)$$

where μ_{NanoH_CoFe} is the spectrum of **NanoH_CoFe**, μ_{H_CoFe} the one of **H_CoFe**, $\mu_{ShellNanoH\_CoFe}$ the one of **ShellNanoH_CoFe**, μ_{NanoH_RbCoFe} the spectrum of **NanoH_RbCoFe**, μ_{H_RbCoFe} the one of **H_RbCoFe**, $\mu_{ShellNanoH\_RbCoFe}$ the one of **ShellNanoH_RbCoFe**, x and y are the contributions of the cores ($0 \leq x \leq 1$; $0 \leq y \leq 1$). This systematic investigation enabled to discard non-physical solutions, and a set of plausible spectra for **ShellNanoH_CoFe** and **ShellNanoH_RbCoFe** could be retained. The 2nd step compared the retained plausible spectra of **ShellNanoH_CoFe** and **ShellNanoH_RbCoFe** together to determine a narrower range for the x and y values. The comparison between the spectra of the two shells showed that for a particular value of x and one of y, the spectrum of **ShellNanoH_CoFe** and of **ShellNanoH_RbCoFe** were very close, as it was the case for **NanoCoFe** and **NanoRbCoFe** in ref. [8]. The room temperature XANES spectra of **NanoH_CoFe** and **NanoH_RbCoFe** are shown in Figure 3a at the Co K-edge and in Figure 3d at the Fe K-edge, the spectra of **H_CoFe** and **H_RbCoFe** in Figure 3b at the Co K-edge and in Figure 3e at the Fe K-edge, and the spectra of **ShellNanoH_CoFe** and **ShellNanoH_RbCoFe** in Figure 3c at the Co K-edge and in Figure 3f at the Fe K-edge. In order to verify i) the reliability of the extracted spectra **ShellNanoH_CoFe** and **ShellNanoH_RbCoFe** and ii) the assumption that the spectra of the cores of **NanoH_CoFe** and **NanoH_RbCoFe** are very close to those of **H_CoFe** and **H_RbCoFe** respectively, a crossed reconstruction of the spectra of the cores of **NanoH_CoFe** and **NanoH_RbCoFe** (**CoreNanoH_CoFe** and **CoreNanoH_RbCoFe**) was done: **CoreNanoH_CoFe** was constructed from the linear combination of **NanoH_CoFe** and **ShellNanoH_RbCoFe** and **CoreNanoH_RbCoFe** was constructed from the linear combination of **NanoH_RbCoFe** and **ShellNanoH_CoFe**. This crossed reconstruction was performed at both edges. The spectra of the reconstructed cores compared to those of the powders **H_**

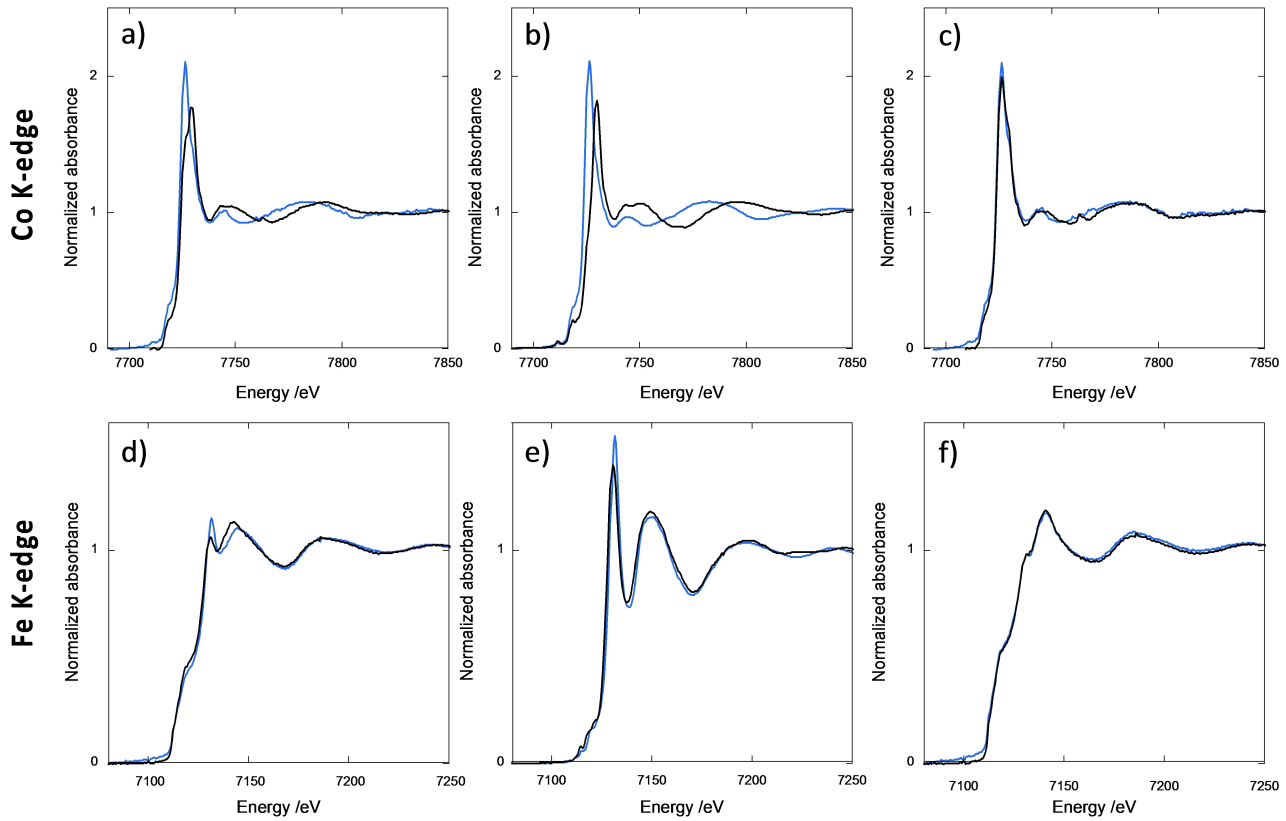

Figure 3. Room temperature XANES spectra at the Co K-edge of a) **NanoH_CoFe** (blue) and **NanoH_RbCoFe** (black), b) of **H_CoFe** (blue) and **H_RbCoFe** (black) and c) of **ShellNanoH_CoFe** (blue) and **ShellNanoH_RbCoFe** (black). Room temperature XANES spectra at the Fe K-edge of d) **NanoH_CoFe** (blue) and **NanoH_RbCoFe** (black), e) of **H_CoFe** (blue) and **H_RbCoFe** (black) and f) of **ShellNanoH_CoFe** (blue) and **ShellNanoH_RbCoFe** (black).

CoFe and **H_RbCoFe** are shown in S5 at both K-edges. The very strong similarity between the spectrum of the powder and of the reconstructed one confirms the reliability of the treatment. From these linear combinations, it appears that the spectra of **NanoH_CoFe** and of **NanoH_RbCoFe** can be decomposed at both edges into two contributions.

One contribution has the same XANES spectra at both edges as the corresponding powders (**CoreNanoH_CoFe** and **CoreNanoH_RbCoFe**). The local environment of the Co and Fe ions is therefore the same as the ones in the corresponding powders. As **NanoH_CoFe** and **NanoH_RbCoFe** exhibit the same diffraction lines at the same angles as the corresponding powders (Figure S1a and S1b), the same local and long range structures strongly suggest that one domain of the nanoparticles is made of the same fcc-$Co^{II}(HS)Fe^{III}$ or fcc-$Co^{III}(LS)Fe^{III}$ phase as the corresponding powder. The other contribution has XANES spectra different from those of the corresponding powders, slightly different at the Co K-edge and strongly different at the Fe K-edge. We propose again to assign the fcc-$Co^{II}(HS)Fe^{III}$ phase to the core of the nanocrystals and the Co and Fe ions, for which the XANES spectra and therefore the local environments deviate from those in the PBA powders, to surface species making the shell of the nanocrystals. On the basis of this analysis, the fcc-$Co^{II}(HS)Fe^{III}$ core of **NanoH_CoFe** is made of 30% of the Co and Fe ions, while the remaining 70% are part of the shell. A scheme for the core-shell structure of the nanocrystals at 300 K is proposed in Figure 4a. This scheme is comparable to the one proposed in ref. [8] for CoFe PBA nanocrystals formed in reaction media different from that used here for **NanoH_CoFe**. Thus, such a core-shell structure appears to be quite general for nanosized CoFe PBA[8] and the peculiar shape of the XANES spectrum at the Fe K-edge is the fingerprint of the distorted $Fe(CN)_6$ entities constituting the outer shell. The effect of the presence of such a shell becomes detectable on the XANES spectra when the surface-to-volume ratio is sufficiently high, which is the case with the 5 nm nanoparticles here.

In a general way, photomagnetic powdered CoFe PBAs are photo-excited by the X-ray beam at the Fe and Co K-edges at

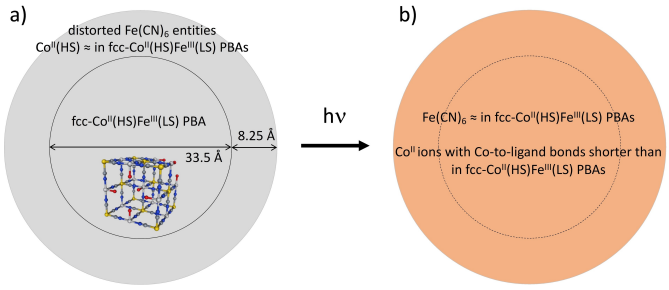

Figure 4. Scheme of the nanocrystals in **NanoH_CoFe** a) at 300 K and b) at 10 K in the photo-excited state.

low temperature and the metastable photo-excited state is the same whether the compound has been irradiated in the visible or in the X-ray spectral range.[13] At 10 K, when exposed to the X-ray beam, the X-ray absorption spectra at the Co and Fe K-edges of **H_CoFe** did not change. The spectra of **H_CoFe** at 10 K after irradiation by the X-ray beam are compared to those recorded at room temperature in S6. This similarity of the spectra before and after irradiation confirms that **H_CoFe** is not photosensitive, as expected for a powdered compound in the fcc-Co^{II}(HS)Fe^{III} ground state. This result is in line with the same temperature dependence of magnetization before and after irradiation in the visible range (Figure 1b). In contrast, as soon as exposed to the X-ray beam, the X-ray absorption spectra at the Co and Fe K-edges of **NanoH_CoFe** started to change till a photo-stationary state was reached after several minutes under irradiation. The XANES spectra at the Co and Fe K-edges of **NanoH_CoFe** at 10 K in the photo-stationary state (also called **Nano_HCoFe*** in the following) are shown in Figure 5, where they are compared to those recorded at room temperature. At both K-edges, the spectra before and after irradiation are different. This result shows that **NanoH_CoFe**, which undergoes a photo-induced transformation under irradiation by visible light at low temperature (Figure 1a and S1), also undergoes a photo-induced transformation under irradiation by the X-ray beam, which is usually observed in photomagnetic PBAs[13] and which was also observed in the case of the nanocrystals **NanoRbCoFe** at the origin of this work.[8] **H_CoFe** being not photoactive, this suggests that the photo-switching properties of **NanoH_CoFe** are specific to the small CoFe PBA particles size.

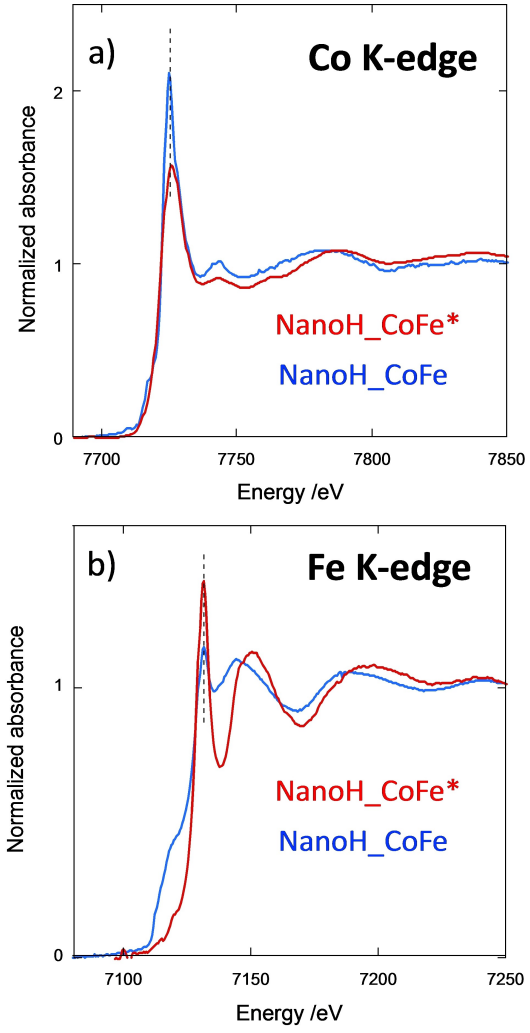

Figure 5. XANES spectra in the ground state at 300 K (blue) and in the photo-stationary state at 10 K (red) of **NanoHCoFe** a) at the Co K-edge and b) at the Fe K-edge.

Whatever the transition metal K-edge, in contrast to those of the ground state, the spectra of **NanoH_CoFe** in the photo-excited state i) resemble those of larger PBA particles mainly made of fcc-Co^{II}(HS)Fe^{III} and ii) cannot be reproduced by any linear combination of model spectra. This was also the case for the photo-induced state of **NanoRbCoFe** in ref. [8], for which the spectra of the ground state could also be reproduced by linear combinations of the spectra of a core and of a shell but not the ones of the photo-excited state.[8] This shows that, either the core-shell structure has completely disappeared in the photo-excited state, or the species making the core and the shell are no more different enough to allow for the extraction of their spectra using linear combinations of model spectra. This is consistent with our recent observation: weak ferromagnetic interaction was detected at the surface of the ferrimagnetic core in the photo-excited state of the $Rb_2Co_4[Fe(CN)_6]_{3.3}\cdot 11H_2O$ powder.[14] This work suggests i) the core-shell structure of the photo-excited state of the powder and ii) very close local structures of the Co and Fe species in the core and in the shell.[14]

Photo-switching of powdered CoFe PBAs is well-documented in the literature and the unique mechanism reported which is at the origin of the photo-induced transformation is the combination of the $Co^{III}Fe^{II}\rightarrow Co^{II}Fe^{III}$ photo-induced electron transfer and the spin conversion of the Co ion. The signature of the $Co^{III}Fe^{II}\rightarrow Co^{II}Fe^{III}$ photo-induced electron transfer on XAS spectra of photo-switchable CoFe PBAs is the shift or the appearance of another absorption maximum on the spectra since the energy of this maximum reflects the oxidation state of the transition metal ions. The single absorption maximum of the XANES spectrum of **NanoH_CoFe** after irradiation (Figure 5) is located at the same energy as before irradiation at both the Co and the Fe K-edges. Contrary to the larger particles, the photo-switching properties in **NanoH_CoFe** are hence not due the $Co^{III}Fe^{II}\rightarrow Co^{II}Fe^{III}$ photo-induced electron transfer.

At the Fe K-edge, the spectrum of the photo-excited state strongly differs from the one of the ground state (Figure 5b); after irradiation it looks like that of **H_CoFe**, i.e. that of $Fe(CN)_6$ entities in CoFe PBA powders made of larger size grains, indicating the presence of $Fe^{III}(CN)_6$ entities in the well-known octahedral environment[2a,4a,12] over the whole nanoparticles volume. The energy of the absorption maximum is in line with $Fe^{III}(CN)_6$ entities. The spectrum at the Fe K-edge of **NanoH_CoFe** in the photo-excited state is compared to that of its core and of its shell at 300 K in Figure 6b. The spectra of **NanoH_CoFe** in the photo-excited state is very close of that of its core in the ground state, but very different to that of its shell. One

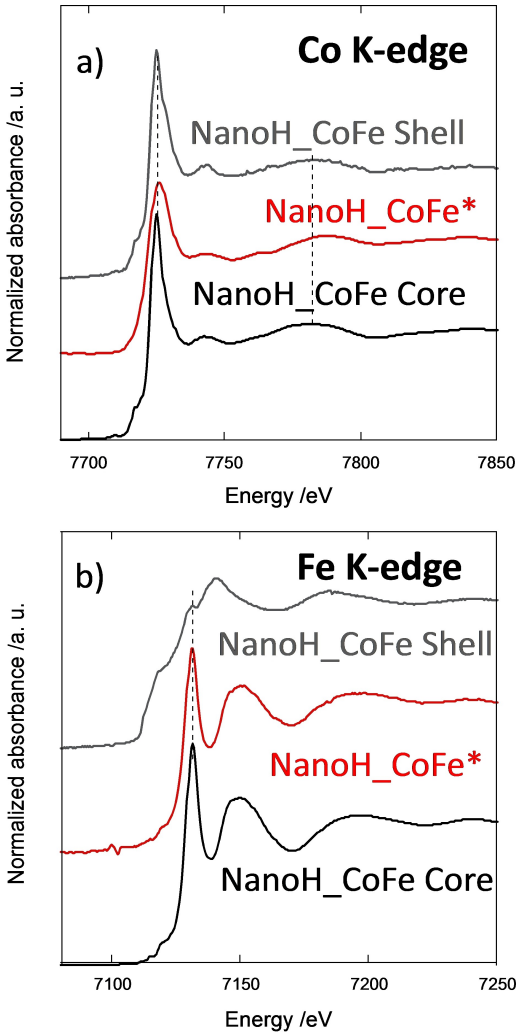

Figure 6. XANES spectra in the ground state at 300 K (blue) and in the photo-stationary state at 10 K (red) of **NanoHCoFe** a) at the Co K-edge and b) at the Fe K-edge.

can conclude that all the Fe^{III} coordination polyhedra, whatever they were part of the core or of the shell in the ground state, adopt the same local structure in the photo-excited state, as in the fcc-$Co^{II}(HS)Fe^{III}$ core. Thus, the Fe species impacted by the photo-induced transformation are essentially those making the shell, the Fe species making the core remaining essentially the same. In **NanoH_CoFe**, this photo-induced transformation cannot result from the photo-induced volume change of the core, which remains in the $Co^{II}Fe^{III}$ state. This photo-induced transformation seems to be specific to the Fe surface species and therefore only observable in particles in which the surface-to-volume ratio is large enough to be detected. A comparable change of the XAS spectrum at the Fe K-edge before and after irradiation was also observed in **NanoRbCoFe** made of a photo-switchable $Co^{III}Fe^{II}$ core.[8]

When comparing the spectra of **NanoH_CoFe** at the Co K-edge before and after irradiation (Figure 5a), it appears that they differ from one another. The first EXAFS oscillation is slightly shifted towards higher energy in the photo-excited state, which reflects slightly shorter Co^{II}-to-ligand bonds in the photo-excited state than in the ground state. Thus, Figure 6a (displaying the spectrum at the Co K-edge of **Nano_HCoFe** after irradiation compared to the spectra of its core and its shell in the ground state) shows that the local structure around the Co^{II} ions, which is very close in the core and the shell of the ground state to the typical one of CoFe PBA powders in the $Co^{II}Fe^{III}$ state, undergoes a slight photo-induced structural transformation associated with a Co-to-ligand bonds shortening over the whole nanocrystals volume. Contrary to the Fe sub-lattice for which the shell species undergo the most spectacular photo-induced transformation, the Co species undergo a comparable photo-induced transformation over the whole nanoparticle's volume, whether they are part of the core or of the shell in the ground state. This suggests that the Co-ligand moieties are part of the photo-active species.

Conclusion

In summary, a peculiar photo-induced transformation, specific to nanosized systems, has been evidenced in **NanoH_CoFe**. This was made possible by synthesizing and investigating nanocrystals, the core of which does not contain the $Co^{III}(LS)Fe^{II}$ pairs well-known to be the photo-switchable species in the larger particles. The photo-induced transformation evidenced in **NanoH_CoFe** is not due to the well-documented photo-induced $Co^{III}(LS)Fe^{II} \rightarrow Co^{II}(HS)Fe^{III}$ electron transfer happening in photomagnetic CoFe PBAs and in the core of PBA nanocrystals with similar chemical composition.[8] It is also not induced by the significant structural change accompanying it. In contrast, the photo-induced transformation of **NanoH_CoFe** mainly impacts the local structure of the transition metal ions with different behaviors of both the Co and Fe sublattices. Such a photo-induced transformation happens whether the core of the nanoparticles exhibits (**NanoRbCoFe** in ref. [8]) or not (**NanoH_CoFe** here) a photomagnetic effect due to the $Co^{III}(LS)Fe^{II} \rightarrow Co^{II}(HS)Fe^{III}$ electron transfer. The photo-switching properties thus appear to be richer and more complex in 5 nm CoFe PBA nanoparticles than in 100 nm ones. The photo-induced transformation, different from the well-documented $Co^{III}(LS)Fe^{II} \rightarrow Co^{II}(HS)Fe^{III}$ electron transfer, occurring whatever the chemical composition of the CoFe PBA nanoparticles, must therefore play a key role in their photo-switching properties. To the best of our knowledge, this is the first evidence of photo-switching properties specific to nanometric size in CoFe PBAs and more generally in nanoparticles of coordination polymers. Work is in progress to finely analyze the structure and the electronic structure of the states involved in these peculiar photo-switching properties and to identify the mechanisms originating them.

Experimental Data

Synthesis of **NanoH_CoFe**, **H_CoFe** and of the two model compounds (called **NanoH_RbCoFe**, and **H_RbCoFe** in the follow-

ing) used to extract the X-ray Absorption Near Edge Spectra (XANES) of the core and of the shell of **NanoH_CoFe**.

Preparation of the $H_3[Fe(CN)_6]_{aq}$ precursor solution: A first solution is prepared by dissolving 10 g (30 mmol) of $K_3[Fe(CN)_6]$ in 150 mL of water. A second aqueous solution is prepared by dissolving 17 g (100 mmol) of $AgNO_3$ in 150 mL of water. The drop-by-drop addition of the silver nitrate solution into the potassium ferricyanide(III) solution produces an orange precipitate constituted of $Ag_3[Fe(CN)_6]$. The powder is centrifuged, washed five times with deionized water to eliminate all solvated ions, and allowed to dry in air.

To obtain the alkali cation free $H_3[Fe(CN)_6]$ aqueous solution, 0.6 M (2.14 g, 4 mmol) of $Ag_3[Fe(CN)_6]$ is solubilized in 5 mL of aqueous hydrochloric acid solution (1.8 M) and stirred for 4 h. The precipitate constituted by AgCl and residual $Ag_3[Fe(CN)_6]_3$ is separated from the $H_3[Fe(CN)_6]$ solution by filtration. The concentration of the $[Fe(CN)_6]^{3-}$ aqueous solution is determined by UV-vis spectroscopy.

Synthesis of NanoH_CoFe and NanoH_RbCoFe

Preparation of monoliths with 2D-hexagonal organization containing cobalt(II) ions with a 0.5% Co^{2+}/Si ratio: The synthesis of the monoliths has already been described elsewhere.[9c] In a typical procedure, a solution is prepared by mixing 2.4 g of P123 with TMOS (26 mmol, 4 g), as a silica precursor, in a 30 mL polypropylene vial. This solution is stirred in a water bath at 50 °C until the P123 copolymer is completely dissolved and then cooled to room temperature. An aqueous cobalt(II) nitrate acidic solution (69 mM, pH 1.4, 2 mL) is then added to the cooled solution. The mixture is stirred for 2 min and 30 seconds and then divided in four vials, which are sealed and transferred into a thermostated water bath at 23 °C to be aged without stirring for 1 h. The samples are left without caps in the water bath at 23 °C for 1 week to give homogeneous pink glassy silica monoliths containing P123 and Co^{2+} ions. Finally, the P123 copolymer is removed by calcination at 500 °C in air.

NanoH_CoFe composite: The synthesis of **NanoH_CoFe** has already been described elsewhere.[11] An impregnating aqueous solution containing $H_3[Fe(CN)_6]$ 0.3 M and HNO_3 0.85 M is prepared. The calcined monoliths containing 0.5% Co^{2+}/Si ions are immersed in heptane (5 mL) and impregnated with a volume of the acidic impregnating solution equal to 80% of the porous volume. After 1 h, the heptane is removed, and the nanocomposites are washed five times with water and air-dried. The nanocomposite is ground before measurements.

NanoH_RbCoFe composite: An impregnating aqueous solution containing $H_3[Fe(CN)_6]$ 0.3 M, HNO_3 0.85 M, and $RbNO_3$ 1.5 M is prepared. The calcined monoliths containing 0.5% Co^{2+}/Si ions are immersed in heptane (5 mL) and impregnated with a volume of the acidic impregnating solution equal to 80% of the porous volume. After 1 h, the heptane is removed, and the nanocomposites are washed five times with water and air-dried. The nanocomposite is ground before measurements.

Synthesis of H_CoFe and H_RbCoFe

H_CoFe: Powder **H_CoFe** is synthesized by addition of 400 mL of a 1.25×10^{-3} M solution of cobalt(II) nitrate hexahydrate to 50 mL of a 10^{-2} M $H_3[Fe(CN)_6]$ aqueous solution. The addition rate is regulated to last 3 h. The powder is centrifuged, washed three times with distilled water, and allowed to dry in air.

H_RbCoFe: Powder **H_RbCoFe** is synthesized by addition of 400 mL of a 1.25×10^{-3} M solution of cobalt(II) nitrate hexahydrate to 50 mL of a 10^{-2} M $H_3[Fe(CN)_6]$ aqueous solution containing 734 mg of $RbNO_3$. The addition rate is regulated to last 3 h. The powder is centrifuged, washed three times with distilled water, and allowed to dry in air.

The powders and nanocomposites were characterized by X-Ray Diffraction (XRD) (S1), IR spectroscopy (S2) and microscopy (S3). All XRD patterns exhibit the peaks of the well-known face-centered structure of PBA. XRD and IR spectroscopy show that **NanoH_CoFe** and **H_CoFe** are mainly made of the $Co^{II}(HS)Fe^{III}$ pairs whereas **NanoH_RbCoFe** and **H_RbCoFe** are mainly made of the $Co^{III}(LS)Fe^{II}$ pairs.

(Photo)-magnetic measurements: Direct Current (DC) data were recorded using a XL-7 SQUID magnetometer. About 10 mg of powder was spread on a piece of cardboard and some drops of nujol oil were added to fixate it. The sample was irradiated at 10 K in the magnetometer with a laser diode (635 nm, 25 mW/cm^2). Field Cooled and Zero-Field Cooled (FC-ZFC) magnetization curves were recorded over the 2–15 K temperature range under a 50 Oe magnetic field.

Samples were irradiated until reaching a photo-stationary state.

XAS measurements: The Co and Fe K-edges spectra were recorded on the SAMBA[15] beamline at synchrotron SOLEIL (Gif-sur-Yvette, France). The Si(220) monochromator in the continuous mode was used to record the spectra. The samples (all as powders) were placed between two Kapton scotch tape and measured in transmission using ionization chambers as detectors. We carefully checked that no radiation damage occurred; at room temperature this was achieved thanks to a defocused beam. At 10 K, the beam was refocused and used to photoexcite the system. The spectra at the Co and Fe K-edges were recorded after heating back to 300 K. They are compared to the spectra recorded at 300 K before cooling and photoexcitation by the X-ray beam in Figure S7. The spectra are the same, showing that the photo-induced transformations are reversible.

The spectra were energy-calibrated and conventionally normalized with the ATHENA software.[16]

Supporting Information

S1 Temperature dependance of the magnetization of **NanoH_CoFe** before and after irradiation; S2 X-ray diffraction patterns of **NanoH_CoFe**, **H_CoFe**, **NanoH_RbCoFe** and **H_RbCoFe**; S3 IR spectra of **NanoH_CoFe**, **H_CoFe**, **NanoH_RbCoFe** and **H_RbCoFe**; S4 Electron microscopy images of the nanocomposite and powders; S5 XANES spectra at the Co and the Fe K-edges of the reconstructed core of **NanoH_CoFe** and **NanoH_RbCoFe** compared to those of the powders; S6 XANES spectra at the Co and Fe K-edges of **H_CoFe** at 300 K and at 10 K after irradiation.

Acknowledgements

We acknowledge SOLEIL for provision of synchrotron radiation through proposal 20211180; we would like to thank G. Alizon for technical support during the experiments. We also would like to

thank E. Rivière for technical support for the (photo)magnetic measurements.

Conflict of Interests

The authors declare no conflict of interest.

Data Availability Statement

The data that support the findings of this study are available from the corresponding author upon reasonable request.

Keywords: photo-switching · Prussian blue analog · nanoparticles · X-ray absorption spectroscopy

[1] O. Sato, T. Iyoda, A. Fujishima, K. Hashimoto, *Science* **1996**, *272*, 704–705.

[2] a) A. Bleuzen, C. Lomenech, V. Escax, F. Villain, F. Varret, C. Cartier dit Moulin, M. Verdaguer, *J. Am. Chem. Soc.* **2000**, *122*, 6648–6652; b) N. Shimamoto, S.-I. Ohkoshi, O. Sato, K. Hashimoto, *Inorg. Chem.* **2002**, *41*, 678–684; c) T. Yokoama, T. Ohta, O. Sato, K. Hashimoto, *Phys. Rev. B* **1998**, *58*, 8257–8266; d) S.-I. Ohkoshi, H. Tokoro, K. Hashimoto, *Coord. Chem. Rev.* **2005**, *249*, 1830–1840; e) H. Tokoro, T. Matsuda, T. Nuida, Y. Moritomo, K. Ohoyama, E. D. Loutete Dangui, K. Boukheddaden, S.-I. Ohkoshi, *Chem. Mater.* **2008**, *20*, 423–428; f) S. Cobo, R. Fernandez, L. Salmon, G. Molnar, A. Bousseksou, *Eur. J. Inorg. Chem.* **2007**, *11*, 1549–1555; g) D. Papanikolaou, S. Margadonna, W. Kosaka, S.-I. Ohkoshi, M. Brunelli, K. Prassides, *J. Am. Chem. Soc.* **2006**, *128*, 8358–8363; h) E. Coronado, M. C. Jimenez-Lopez, T. Korzeniak, G. Levchenko, F. M. Romero, A. Segura, V. Garcia-Baonza, J. C. Cezar, F. M. F. de Groot, A. Milner, M. Paz-Pasternak, *J. Am. Chem. Soc.* **2008**, *130*, 15519–15532; i) C. Avendano, M. G. Hilfiger, A. Prosvirin, C. Sanders, D. Stepien, K. R. Dunbar, *J. Am. Chem. Soc.* **2010**, *132*, 13123–13125; j) Y. Arimoto, S. I. Ohkoshi, Z. J. Zhong, H. Seino, Y. Mizobe, K. Hashimoto, *J. Am. Chem. Soc.* **2003**, *125*, 9240–9241; k) S. I. Ohkoshi, S. Ikeda, T. Hozumi, T. Kashiwagi, K. Hashimoto, *J. Am. Chem. Soc.* **2006**, *128*, 5320–5321; l) S.-I. Ohkoshi, H. Tokoro, T. Hozumi, Y. Zhang, K. Hashimoto, C. Mathonière, I. Bord, G. Rombaut, M. Verelst, C. Cartier dit Moulin, F. Villain, *J. Am. Chem. Soc.* **2006**, *128*, 270–277; m) T. Hozumi, K. Hashimoto, S. I. Ohkoshi, *J. Am. Chem. Soc.* **2005**, *127*, 3864–3869; n) J.-D. Cafun, G. Champion, M.-A. Arrio, C. Cartier dit Moulin, A. Bleuzen, *J. Am. Chem. Soc.* **2010**, *132*, 11552–11559; o) J.-D. Cafun, J. Lejeune, F. Baudelet, P. Dumas, J.-P. Itié, A. Bleuzen, *Angew. Chem. Int. Ed.* **2012**, *51*, 9146–9148; p) M. Cammarata, S. Zerdane, L. Balducci, G. Azzolina, S. Mazerat, C. Exertier, M. Trabuco, M. Levantino, R. Alonso-Mori, J. M. Glownia, S. Song, L. Catala, T. Mallah, S. F. Matar, E. Collet, *Nat. Chem.* **2021**, *13*, 10–14.

[3] a) J. M. Herrera, V. Marvaud, M. Verdaguer, J. Marrot, M. Kalisz, C. Mathonière, *Angew. Chem. Int. Ed.* **2004**, *43*, 5468–5471; b) C. P. Berlinguette, A. Dragulescu-Andrasi, A. Sieber, J. R. Galan-Mascaros, H. U. Güdel, C. Achim, K. R. Dunbar, *J. Am. Chem. Soc.* **2004**, *126*, 6222–6223; c) M. Shatruk, A. Dragulescu-Andrasi, K. E. Chambers, S. A. Stoian, E. L. Bominaar, C. Achim, K. R. Dunbar, *J. Am. Chem. Soc.* **2007**, *129*, 6104–6116; d) D. Li, R. Clérac, O. Roubeau, E. Harte, C. Mathonière, R. Le Bris, S. M. Holmes, *J. Am. Chem. Soc.* **2008**, *130*, 252–257; e) Y. Zhang, D. Li, R. Clérac, M. Kalisz, C. Mathonière, S. Holmes, *Angew. Chem. Int. Ed.* **2010**, *49*, 3752–3756; f) M. Nihei, Y. Sekine, N. Suganami, K. Nakasawa, H. Nakao, Y. Murakawi, H. Oshio, *J. Am. Chem. Soc.* **2011**, *133*, 3592–3600; g) M. Nihei, Y. Okamoto, Y. Sekine, N. Hoshino, T. Shiga, I. Po-Chun Liu, H. Oshio, *Angew. Chem. Int. Ed.* **2012**, *51*, 6361–6364; h) T. Liu, D.-P. Dong, S. Kanegawa, S. Kang, O. Sato, Y. Shiota, K. Yoshizawa, S. Hayami, S. Wu, C. He, C.-Y. Duan, *Angew. Chem. Int. Ed.* **2012**, *51*, 4367–4370; i) A. Mondal, Y. Li, M. Seuleiman, M. Julve, L. Toupet, M. Buron-Le Cointe, R. Lescouezec, *J. Am. Chem. Soc.* **2013**, *135*, 1653–1656; j) A. Mondal, L.-M. Chamoreau, Y. Li, Y. Journaux, M. Seuleiman, R. Lescouezec, *Chem. Eur. J.* **2013**, *19*, 7682–7685; k) E. S. Koumousi, I.-R. Jeon, Q. Gao, P. Dechambenoit, D. N. Woodruff, P. Merzeau, L. Buisson, X. Jia, D. Li, F. Volatron, C. Mathonière, R. Clérac, *J. Am. Chem. Soc.* **2014**, *136*, 15461–15464; l) D. Garnier, J.-R. Jimenez, Y. Li, J. von Bardeleben, Y. Journaux, T. Augenstein, E. M. B. Moos, M. T. Gamer, F. Breher, R. Lescouezec, *Chem. Sci.* **2016**, *7*, 4825–4831; m) B. P. Macpherson, P. V. Bernhardt, A. Hauser, S. Pages, E. Vauthey, *Inorg. Chem.* **2005**, *44*, 5530–5536.

[4] a) C. Cartier dit Moulin, F. Villain, A. Bleuzen, M.-A. Arrio, P. Sainctavit, C. Lomenech, V. Escax, F. Baudelet, E. Dartyge, J.-J. Gallet, M. Verdaguer, *J. Am. Chem. Soc.* **2000**, *122*, 6653–6658; b) V. Escax, A. Bleuzen, J. P. Itié, P. Münsch, F. Varret, M. Verdaguer, *J. Phys. Chem. B* **2003**, *107*, 4763–4767.

[5] A. Lüdi, H. U. Güdel, *Structure and Bonding*, Springer-Verlag, Berlin **1973**, pp 1–21.

[6] a) L. Catala, C. Mathonière, A. Gloter, O. Stéphan, T. Gacoin, J.-P. Boilot, T. Mallah, *Chem. Commun.* **2005**, 746–748; b) F. Volatron, D. Heurtaux, L. Catala, C. Mathonière, A. Gloter, O. Stéphan, D. Repetto, M. Clemente-Leon, E. Coronado, T. Mallah, *Chem. Commun.* **2011**, *47*, 1985–1987; c) D. Brinzei, L. Catala, C. Mathonière, W. Wernsdorfer, A. Gloter, O. Stephan, T. Mallah, *J. Am. Chem. Soc.* **2007**, *129*, 3778–3779; d) J. G. Moore, E. J. Lochner, C. Ramsey, N. S. Dalal, A. E. Stiegman, *Angew. Chem. Int. Ed.* **2003**, *42*, 2741–2743; e) G. Fornasieri, A. Bleuzen, *Angew. Chem. Int. Ed.* **2008**, *47*, 7750–7752; f) P. Durand, G. Fornasieri, C. Baumier, P. Beaunier, D. Durand, E. Rivière, A. Bleuzen, *J. Mater. Chem.* **2010**, *20*, 9348–9354; g) D. M. Pajerowski, F. A. Frye, D. R. Talham, M. W. Meisel, *New J. Phys.* **2007**, *9*, 222–226; h) L. Trinh, S. Zerdane, S. Mazeŕat, N. Dia, D. Dragoe, C. Herrero, E. Rivier`e, L. Catala, M. Cammarata, E. Collet, T. Mallah, *Inorg. Chem.* **2020**, *59*, 13153–13161.

[7] S. Brossard, F. Volatron, L. Lisnard, M.-A. Arrio, L. Catala, C. Mathonière, T. Mallah, C. Cartier dit Moulin, A. Rogalev, F. Wilhelm, A. Smekhova, P. Sainctavit, *J. Am. Chem. Soc.* **2012**, *134*, 222–228.

[8] A. Bordage, R. Moulin, E. Fonda, G. Fornasieri, E. Rivière, A. Bleuzen, *J. Am. Chem. Soc.* **2018**, *140(32)*, 10332–10343.

[9] a) P. Durand, G. Fornasieri, C. Baumier, P. Beaunier, D. Durand, E. Rivière, A. Bleuzen, *J. Mater. Chem.* **2010**, *20*, 9348–9354; b) M. Aouadi, G. Fornasieri, V. Briois, P. Durand, A. Bleuzen, *Chem. Eur. J.* **2012**, *18*, 2617–2623; c) E. Delahaye, R. Moulin, M. Aouadi, V. Trannoy, P. Beaunier, G. Fornasieri, A. Bleuzen, *Chem. Eur. J.* **2015**, *21*, 16906–16916; d) G. Fornasieri, A. Bordage, A. Bleuzen, *Eur. J. Inorg. Chem.* **2018**, *3–4*, 259–271; e) L. Altenschmidt, G. Fornasieri, E. Rivière, F. Brisset, R. Saint-Martin, A. Bleuzen, *C. R. Chim.* **2019**, *22*, 508–515.

[10] G. Fornasieri, M. Aouadi, P. Durand, P. Beaunier, E. Rivière, A. Bleuzen, *Chem. Commun.* **2010**, *46*, 8061–8063.

[11] A. Bleuzen, M. Goncalves, L. Altenschmidt, G. Fornasieri, A. Bordage, E. Rivière, *Chem. Sq.* **2020**, *4*, 1.

[12] a) V. Escax, A. Bleuzen, C. Cartier dit Moulin, F. Villain, A. Goujon, F. Varret, M. Verdaguer, *J. Am. Chem. Soc.* **2001**, *123*, 12536–12543; b) T. Yokoyama, T. Ohta, O. Sato, K. Hashimoto, *Phys. Rev. B* **1999**, *58*, 8257–8266; c) T. Yokoyama, M. Kigushi, T. Ohta, O. Sato, Y. Einaga, K. Hashimoto, *Phys. Rev. B* **1999**, *60*, 9340–9346.

[13] a) R. Moulin, E. Delahaye, A. Bordage, E. Fonda, J.-P. Baltaze, P. Beaunier, E. Rivière, G. Fornasieri, A. Bleuzen, *Eur. J. Inorg. Chem.* **2017**, *10*, 1303–1313; b) J.-D. Cafun, J. Lejeune, F. Baudelet, P. Dumas, J.-P. Itié, A. Bleuzen, *Angew. Chem. Int. Ed.* **2012**, *51*, 9146–9148.

[14] S. F. Jafri, M.-A. Arrio, A. Bordage, R. Moulin, A. Juhin, C. Cartier dit Moulin, E. Otero, P. Ohresser, A. Bleuzen, P. Sainctavit, *Inorg. Chem.* **2018**, *57*, 7610–7619.

[15] V. Briois, E. Fonda, S. Belin, L. Bathe, C. La Fontaine, F. Langlois, M. Ribbens, F. Villain, *UVX2010* **2011**, 41–47.

[16] B. Ravel, M. Newville, *J. Synchrotron Radiat.* **2005**, *12*, 537–541.

Manuscript received: May 23, 2023
Accepted manuscript online: June 7, 2023
Version of record online: June 26, 2023